Supramolecular Structure in Full-Length Alzheimer's β-Amyloid Fibrils: Evidence for a Parallel β-Sheet Organization from Solid-State Nuclear Magnetic Resonance

John J. Balbach,* Aneta T. Petkova,* Nathan A. Oyler,* Oleg N. Antzutkin,† David J. Gordon,‡ Stephen C. Meredith,§ and Robert Tycko*

*Laboratory of Chemical Physics, the National Institute of Diabetes and Digestive and Kidney Diseases, the National Institutes of Health, Bethesda, Maryland 20892-0520 USA; †Division of Inorganic Chemistry, Luleå University of Technology, Luleå, Sweden; and ‡Department of Biochemistry and Molecular Biology and §Department of Pathology, The University of Chicago, Chicago, Illinois 60637 USA

ABSTRACT We report constraints on the supramolecular structure of amyloid fibrils formed by the 40-residue β-amyloid peptide associated with Alzheimer's disease ($A\beta_{1-40}$) obtained from solid-state nuclear magnetic resonance (NMR) measurements of intermolecular dipole-dipole couplings between ^{13}C labels at 11 carbon sites in residues 2 through 39. The measurements are carried out under magic-angle spinning conditions, using the constant-time finite-pulse radiofrequency-driven recoupling (fpRFDR-CT) technique. We also present one-dimensional ^{13}C magic-angle spinning NMR spectra of the labeled $A\beta_{1-40}$ samples. The fpRFDR-CT data reveal nearest-neighbor intermolecular distances of 4.8 ± 0.5 Å for carbon sites from residues 12 through 39, indicating a parallel alignment of neighboring peptide chains in the predominantly β-sheet structure of the amyloid fibrils. The one-dimensional NMR spectra indicate structural order at these sites. The fpRFDR-CT data and NMR spectra also indicate structural disorder in the N-terminal segment of $A\beta_{1-40}$, including the first nine residues. These results place strong constraints on any molecular-level structural model for full-length β-amyloid fibrils.

INTRODUCTION

Amyloid fibrils are filamentous structures formed by a variety of peptides and proteins with widely disparate lengths and amino acid sequences (Sunde and Blake, 1998). Interest in the molecular structure of amyloid fibrils stems from their involvement in amyloid diseases and from the experimental but still mysterious fact that the amyloid fibril is a stable state of a very large (perhaps almost universal) class of polypeptides under appropriate conditions (Chiti et al., 1999). Various experimental techniques permit the characterization of amyloid fibril structures at various levels of resolution. X-ray diffraction measurements on aligned fibril bundles indicate the predominance of a "cross-β" structure for all amyloid fibrils (Inouye et al., 1993; Malinchik et al., 1998; Blake and Serpell, 1996; Sunde et al., 1997; Serpell et al., 2000), in which β-strand segments in fibril-forming peptides and proteins associate into highly extended (microns in length) β-sheet ribbons with the peptide chains running nearly perpendicular to and the intermolecular hydrogen bonds running nearly parallel to the long axis of the fibril. Electron microscopy (EM) permits the visualization of the morphology of amyloid fibrils with a resolution of several nanometers (Fraser et al., 1991, 1992). Higher-resolution and three-dimensional structural features are available from cryo-EM measurements (Jimenez et al., 1999; Serpell and Smith, 2000). Scanning transmission electron microscopy (Goldsbury et al., 2000; O. N. Antzutkin, R. D. Leapman, N. W. Rizzo, J. J. Balbach, and R. Tycko. 2002, submitted manuscript) and neutron scattering (Burkoth et al., 2000) permit the determination of the mass-per-length of fibrils, which places constraints on their supramolecular structure. Atomic force microscopy provides morphological information similar to that from EM, but with the additional capability of monitoring fibril formation in situ (Stine et al., 1996; Harper et al., 1997, 1999; Goldsbury et al., 1999; Blackley et al., 2000).

Molecular-level details of amyloid fibril structures are accessible from solid-state nuclear magnetic resonance (NMR) measurements (Lansbury et al., 1995; Griffiths et al., 1995; Costa et al., 1997; Gregory et al., 1998; Benzinger et al., 1998, 2000; Burkoth et al., 2000; Balbach et al., 2000; Antzutkin et al., 2000; Tycko, 2000, 2001a,b; Ishii et al., 2001b; O. N. Antzutkin, R. D. Leapman, N. W. Rizzo, J. J. Balbach, and R. Tycko, submitted manuscript; A. T. Petkova, Y. Ishii, O. N. Antzutkin, J. J. Balbach, R. D. Leapman, and R. Tycko, submitted manuscript). Information available from solid-state NMR includes the structural organization of β-sheets (e.g., parallel or antiparallel), the identification of β-strand segments and of other secondary structure elements, the identification of structurally ordered and structurally disordered regions within the amino acid sequence of the fibrillized peptide or protein, and the characterization of the molecular conformation and intermolecular contacts within amyloid fibrils. Solid-state NMR studies of amyloid fibrils by several groups have shown that amyloid fibrils are amenable to quite sophisticated spectroscopic techniques (Lansbury et al., 1995; Gregory et al., 1998; Balbach et al., 2000; Antzutkin et al., 2000; Ishii et al., 2001b).

Submitted December 19, 2001, and accepted for publication April 4, 2002.

Address reprint requests to Dr. Robert Tycko, National Institutes of Health, Building 5, Room 112, Bethesda, MD 20892-0520; Tel.: 301-402-8272; Fax: 301-496-0825; E-mail: tycko@helix.nih.gov.

0006-3495/02/08/1205/12 $2.00

In this paper, we report a series of solid-state NMR measurements to characterize the supramolecular organization, in particular the intermolecular alignment of peptide chains within β-sheet units, in fibrils formed by the β-amyloid peptide associated with Alzheimer's disease (Aβ). In vivo, full-length Aβ exists as heterogeneous mixture of peptides ranging from 39 to 43 residues in length due to variations in the C-terminal γ-secretase site (Storey and Cappai, 1999). Experiments described below are performed on the 40-residue peptide ($A\beta_{1-40}$), prepared synthetically to permit ^{13}C labeling of specific carbon sites. The measurements use the constant-time, finite-pulse radiofrequency-driven recoupling (fpRFDR-CT) technique recently developed by Ishii et al. (2001a) to measure ^{13}C-^{13}C magnetic dipole-dipole couplings and hence carbon-carbon distances. Data are reported for $A\beta_{1-40}$ samples in which single ^{13}C labels are introduced at a total of 11 positions across the entire peptide sequence. The fpRFDR-CT data reveal nearest-neighbor intermolecular distances of 4.8 $\pm$ 0.5 Å between ^{13}C labels, indicating a structurally ordered in-register parallel alignment of $A\beta_{1-40}$ chains in the fibrils that encompasses residues 12 through 39. The data also show that the N-terminal segment of $A\beta_{1-40}$, including the first nine residues, is structurally disordered in the fibrils. Disorder in the N-terminal segment is supported by linewidths in one-dimensional ^{13}C NMR spectra. The fpRFDR-CT data reinforce and extend our earlier multiple quantum ^{13}C NMR measurements on $A\beta_{1-40}$ fibrils (Antzutkin et al., 2000), which established that alanine residues at positions 21 and 30, but not position 2, in the amino acid sequence are contained in extended, in-register parallel β-sheets. Our fpRFDR-CT data for $A\beta_{1-40}$ fibrils are similar to DRAWS (Dipolar Recoupling with A Windowless Sequence) dipolar recoupling data reported by Lynn, Meredith, Botto, and coworkers for fibrils formed by residues 10 to 35 of the β-amyloid peptide ($A\beta_{10-35}$), which demonstrated an in-register parallel β-sheet organization in $A\beta_{10-35}$ fibrils (Gregory et al., 1998; Benzinger et al., 1998, 2000; Burkoth et al., 2000).

As a necessary methodological sidelight, the sensitivity of fpRFDR-CT measurements to effects of ^{13}C chemical shift anisotropy (CSA) and transverse spin relaxation is also investigated in this paper through a series of numerical simulations. The simulations demonstrate the robustness of fpRFDR-CT measurements with respect to CSA and spin relaxation, in support of our use of this technique as a structural probe of amyloid fibrils.

MATERIALS AND METHODS

Peptide synthesis and fibrillization

Peptides with the human $A\beta_{1-40}$ sequence DAEFRHDSGY EVHHQKLVFF AEDVGSNKGA IIGLMVGGVV were synthesized and purified as previously described (Antzutkin et al., 2000; Benzinger et al., 2000). Fibrillization was carried out by incubation of aqueous solutions of purified $A\beta_{1-40}$ at ~1 mM peptide concentration, pH $\approx$ 7.4, and room temperature with 0.01% w/v NaN_3 to inhibit bacterial and fungal growth. Incubating solutions were unbuffered, and the pH was monitored approximately daily and adjusted by dropwise addition of dilute NaOH or acetic acid. Solutions were incubated for 14 to 21 days, with gentle rocking, and then lyophilized for solid-state NMR measurements. Preparation of samples in which >80% of the peptide molecules were contained in amyloid fibrils, rather than in nonfibrillar aggregates, was confirmed by EM measurements on selected samples and by the observation of characteristic features of the natural-abundance ^{13}C signals in one-dimensional magic-angle spinning (MAS) NMR spectra of all samples (Antzutkin et al., 2000) and by the linewidths of ^{13}C NMR signals arising from the ^{13}C labels (see below). Samples that were found not to be fully fibrillized after initial incubation were refibrillized by dialysis of the lyophilized peptide against 0.01% w/v NaN_3, pH $\approx$ 7.4 for an additional 7 to 14 days. Fibrillized sample quantities for solid-state NMR measurements were 3 to 10 mg. Unfibrillized samples, used as controls, were prepared by lyophilization of purified $A\beta_{1-40}$ without incubation.

$A\beta_{1-40}$ samples were synthesized with ^{13}C labels at single backbone carbonyl or β-carbon sites. A single sample was prepared with ^{13}C labels at both the carbonyl site of Val-12 and the α-carbon site of Gly-9.

To investigate possible effects of ionic strength on β-sheet organization in $A\beta_{1-40}$ fibrils, one sample was prepared by incubation in phosphate-buffered saline (140 mM NaCl, 3 mM KCl, 10 mM phosphate, pH 7.4) at a peptide concentration of 50 μM. This sample was ^{13}C-labeled at the carbonyl site of Val-39. After incubation and lyophilization, this sample was dialyzed for 1 day to remove excess salt and lyophilized again. Data for this sample are shown in Figs. 2 *c* and 3 *c* (+ symbols; see Figs. 2 and 3). All other incubation solutions were at low ionic strength, as described above.

Solid-state NMR spectroscopy

Solid-state NMR data were acquired at ^{13}C NMR frequencies of 100.4 and 100.8 MHz, using Varian/Chemagnetics Infinity-400 spectrometers and Varian/Chemagnetics MAS probes with 3.2-mm rotors. All measurements were performed at room temperature. One-dimensional ^{13}C NMR spectra were acquired at MAS frequencies ν_R between 10.0 and 20.0 kHz, using standard cross-polarization and high-power proton decoupling techniques. Typically, 3600 or more scans were required to achieve adequate signal-to-noise for the natural-abundance ^{13}C signals from a 10-mg $A\beta_{1-40}$ sample. Spectra in Fig. 2 were obtained with varying numbers of scans, depending on the sample size, the linewidths, and the final signal-to-noise ratio (see Fig. 2).

The fpRFDR-CT technique used in this study is an example of a dipolar recoupling technique, i.e., a radiofrequency (rf) pulse sequence that is applied in synchrony with MAS to restore nuclear magnetic dipole-dipole couplings that are otherwise averaged to zero by MAS, thereby permitting structural measurements while preserving the sensitivity and resolution advantages of MAS (Tycko and Dabbagh, 1990; Griffin, 1998; Gullion and Schaefer, 1989). The fpRFDR-CT data were acquired as described by Ishii et al. (2001a). The fpRFDR-CT measurements make use of an RFDR sequence (Gullion and Vega, 1992; Bennett et al., 1992, 1998) (one ^{13}C π pulse per MAS rotor period, with XY-16 phase incrementation (Gullion et al., 1990)) to recouple homonuclear ^{13}C-^{13}C dipole-dipole interactions but in the limit of high-speed MAS where the recoupling mechanism is provided by finite-pulse effects rather than by chemical shift modulation of the dipole-dipole interactions. As shown by Ishii (2001), the average homonuclear dipole-dipole coupling under fpRFDR has the same operator form as a static dipole-dipole coupling, allowing multiple pulse sequences originally designed for static samples to be applied to rotating samples under high-speed MAS. In fpRFDR-CT, the fpRFDR sequence is inserted into

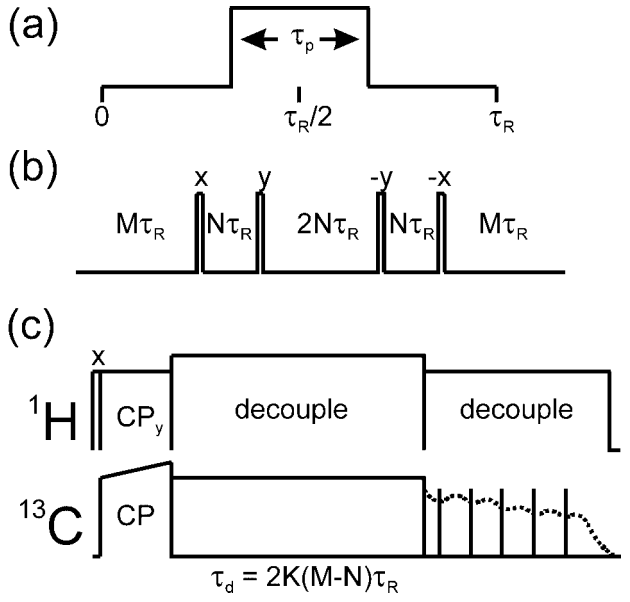

FIGURE 1 Radiofrequency pulse sequence for fpRFDR-CT measurements. (*a*) Finite-pulse radiofrequency-driven recoupling (fpRFDR) sequence consists of a train of π pulses of length τ_p centered in the MAS rotation period τ_R, resulting in an average ^{13}C-^{13}C dipole-dipole coupling Hamiltonian under MAS with the same operator form as a static dipole-dipole coupling (Ishii; 2001; Ishii et al., 2001a). The magnitude of the effective coupling depends on τ_p/τ_R. (*b*) Pulse cycle of length $2(M + 2N)\tau_R$ is constructed from four $\pi/2$ pulses with the indicated phases, separated by integral multiples of τ_R during which the fpRFDR sequence is applied. The average coupling is scaled by $(M - N)/(M + 2N)$. (*c*) Full pulse sequence includes cross-polarization (CP) from ^1H nuclei to ^{13}C nuclei, a constant-time (CT) dipolar evolution period (*shaded box*), and a detection period during which ^{13}C NMR signals (*dashed line*) are digitized in intervals between spin locking pulses. During the evolution period, K repetitions of the pulse cycle in part *b* are applied. The fpRFDR-CT curves in Fig. 3 are generated by varying M and N while keeping $M + 2N$ constant, resulting in the variable effective evolution time τ_d.

the delays between $\pi/2$ pulses in a four-pulse WAHUHA cycle (Haeberlen and Waugh, 1968), as shown in Fig. 1. When the numbers of rotor periods M and N (Fig. 1) in these delays are equal, the WAHUHA cycle averages the homonuclear couplings to zero. When $M \neq N$, the homonuclear couplings are scaled by a factor $(M - N)/(M + 2N)$. Thus, by incrementing M and decrementing N, the effective coupling strengths over the complete WAHUHA cycle can be incremented while maintaining a constant cycle time $2(M + 2N)\tau_R$, in which τ_R is the rotor period. Equivalently, the effective dipolar evolution time $\tau_d \equiv 2K(M - N)\tau_R$ can be incremented while maintaining a constant pulse sequence duration $2K(M + 2N)\tau_R$, in which K is the number of WAHUHA cycles. The constant-time nature of the fpRFDR-CT technique reduces the sensitivity of the data to effects of spin relaxation and pulse imperfections.

In the experiments reported below, fpRFDR-CT data were acquired with $\tau_R = 50$ μs and with π pulse lengths of 15 μs. M was incremented from 64 to 184 in increments of 8, whereas N was decremented from 64 to 4 in decrements of 4, with $K = 4$, leading to τ_d values from 0.0 to 72.0 ms with increments of 4.8 ms. In the case of fpRFDR-CT measurements on the α-carbon of Gly-9, $K = 2$ and τ_d consequently ranged from 0.0 to 36.0 ms with increments of 2.4 ms. In all fpRFDR-CT measurements, the ^{13}C rf carrier frequency was set to the NMR frequency of the ^{13}C-labeled site. As confirmed by numerical simulations, the dipolar recoupling effect of the fpRFDR sequence has sufficient frequency selectivity under the conditions of our experiments that dipolar evolution curves could be recorded separately for the carbonyl carbon of Val-12 and the α-carbon of Gly-9 in the same doubly labeled sample.

The signal-to-noise ratio of fpRFDR-CT measurements was enhanced by pulsed spin-lock detection, as previously described (Petkova and Tycko, 2002). Briefly, a train of ^{13}C pulses with flip angles of ~150° and rotor synchronized spacings of 1.0 ms was applied during the detection period (Fig. 1 *c*), with ^{13}C NMR signals digitized in the delays between pulses. The pulsed spin-lock technique extended the ^{13}C free induction decay significantly, resulting in effective linewidths of ~30 Hz. For a fixed number of scans, the signal-to-noise ratio in the fpRFDR-CT data was thereby increased by a factor of $\xi \approx \sqrt{LW/30}$, in which LW is the linewidth in the absence of pulsed spin-lock. For a fixed delay between scans, the time required to reach a desired signal-to-noise was reduced by a factor of ξ^2. In these experiments, ξ was ~2.5 to 4.7, depending on the ^{13}C-labeled site.

Delays between scans in fpRFDR-CT measurements were 4 s. This value was chosen to minimize probe heating due to the relatively long (76.8-ms) recoupling periods and long (~70-ms) pulsed spin-lock detection periods in the measurements. All measurements were performed nominally at room temperature. No signs of significant sample heating, such as detuning of the NMR probe during measurements, were detected.

Transverse ^{13}C spin relaxation times were measured under MAS at $\nu_R = 20.0$ kHz, using a Carr-Purcell multiple echo sequence (Carr and Purcell, 1954). The interval between π pulses in the Carr-Purcell sequence was set to 200 μs, corresponding to $4\tau_R$. Echo signals were digitized between each pair of π pulses, resulting in a one-dimensional signal decay curve. Proton decoupling fields during the Carr-Purcell sequence were 120 kHz, and ^{13}C π pulse lengths were typically 7 μs. ^{13}C magnetization was prepared along the rotating frame x axis by cross-polarization, and π pulse phases alternated between $+y$ and $-y$ to prevent spin locking and to minimize effects of rf field inhomogeneity on the experimental echo decays. Echo decays $E(t)$ could be fit well to the form $E(t)/E(0) = f_a \exp(-t/T_{2a}) + f_b \exp(-t/T_{2b})$,i.e., to the sum of two decaying exponentials with fractional amplitudes f_a and f_b. The Carr-Purcell data could not be fit adequately by a single exponential decay. Uncertainty in measured T_{2a} and T_{2b} values was approximately ±10%.

Simulations of solid-state NMR data

Simulations of fpRFDR-CT experiments were performed with Fortran programs written specifically for this purpose and were executed on a personal computer with dual Pentium III 900 MHz processors. Three types of simulations of the evolution of the nuclear spin density matrix were performed. All simulations included orientational averaging to mimic the experimental condition of an unoriented powder sample. The number of spins included in the three types of simulations differed because of processing time considerations. For determination of the ^{13}C-^{13}C distances in amyloid fibrils (see Fig. 4 *a*), simulations were carried out for a linear chain of six dipole-coupled ^{13}C spins, including couplings among all spins (i.e., not only the nearest-neighbor couplings). These simulations were carried out at the average Hamiltonian level, i.e., assuming that the fpRFDR-CT pulse sequence creates an ideal, time-independent effective dipole-dipole coupling and that all other interactions are negligible, using the average Hamiltonian given explicitly by Ishii et al. (2001a). For investigation of the effects of CSA on fpRFDR-CT dephasing curves (see Fig. 4 *b*), simulations were carried out for a coupled four-spin system with full numerical evaluation of the spin evolution operator under the pulse sequence. The continuously time-dependent nuclear spin Hamiltonian under MAS, including the dipole-dipole coupling, CSA, and rf field terms, was approximated by a piecewise-constant Hamiltonian, with a time step $\delta t = \tau_R/32$. The symmetry of the fpRFDR pulse sequence simplified and accelerated these simulations by permitting the full evolution operator to be calculated

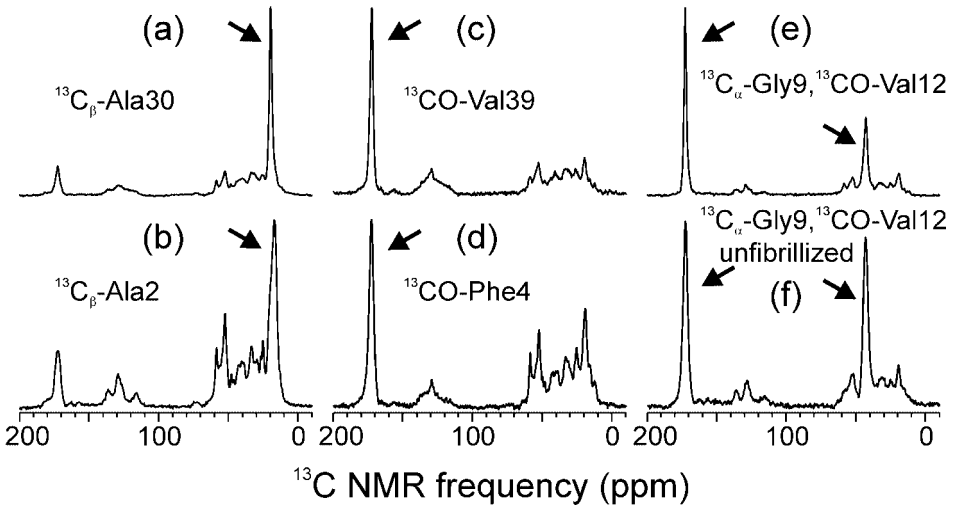

FIGURE 2 Representative one-dimensional ^{13}C NMR spectra of Aβ_{1-40} samples with ^{13}C labels at the indicated sites. Arrows indicate the NMR lines of the labeled sites. Other signals are from natural-abundance ^{13}C at aliphatic (10–60 ppm), aromatic (110–140 ppm), and carbonyl and carboxyl (168–185 ppm) sites. Spectra are obtained at a ^{13}C NMR frequency of 100.8 MHz, with cross-polarization, proton decoupling fields of 100 to 120 kHz, and MAS frequencies of 10.0 kHz (*a* and *b*) or 20.0 kHz (*c*, *d*, *e*, *f*). All Aβ_{1-40} samples are fibrillized by incubation of unbuffered aqueous solutions at pH 7.4, low ionic strength, and ~1 mM peptide concentrations except samples in part *c* (50 μM peptide concentration, phosphate-buffered saline) and part *f* (purified and lyophilized without incubation).

from the evolution operator for a single rotation period. Finally, for investigation of the effects of nuclear spin relaxation on fpRFDR-CT data (Fig. 4, *c* and *d*), simulations were carried out for a coupled two-spin system, with explicit evaluation of the time-dependence of the spin density matrix under the full rf pulse sequence and with inclusion of transverse spin relaxation by multiplication of each off-diagonal density matrix element by $1 - \exp(-|\Delta m|\delta t/T_2)$ after each time step, in which T_2 is the transverse relaxation time and Δm is the multiple quantum coherence order of the off-diagonal element (i.e., the net number of spin flips). This use of a relaxation rate proportional to Δm is a consequence of the assumption that transverse relaxation arises from fluctuating fields with identical amplitudes and correlation times at each ^{13}C site and with no correlations between different sites. The treatment of transverse relaxation by damping the off-diagonal density matrix elements after each time step δt is strictly valid when the correlation time of the fluctuating fields is short compared with δt. When the correlation time is comparable with or larger than δt, this treatment of transverse relaxation is an approximation.

RESULTS

One-dimensional ^{13}C NMR spectra

Fig. 2 shows one-dimensional (1D) ^{13}C MAS NMR spectra of several of the Aβ_{1-40} samples examined in this work. Significant variations in ^{13}C NMR linewidths (full-width at half maximum) for labeled sites are observed in fibrillized Aβ_{1-40} samples, depending on the position of the ^{13}C label. Linewidths in unfibrillized samples are significantly greater than in fibrillized samples. Linewidth data are summarized in Table 1. Compared with unfibrillized samples, fibrillized samples exhibit a pronounced sharpening of natural-abundance aliphatic ^{13}C NMR signals in the 10 to 60 ppm region of the MAS spectrum, especially the development of a peak at 58 ppm attributable to a subset of the natural-abundance α-carbons. This peak serves as an empirical signature of nearly complete fibrillization of Aβ_{1-40} and related β-amyloid peptides (Antzutkin et al., 2000; O. N. Antzutkin, R. D. Leapman, N. W. Rizzo, J. J. Balbach, and R. Tycko. 2002, submitted manuscript). (Apparent differences in the natural-abundance aromatic ^{13}C NMR signals (110–140 ppm, Fig. 2, *a–d*) are due largely to background signals from the NMR probe and MAS rotor.)

TABLE 1 ^{13}C NMR linewidths (FWHM) for labeled sites in fibrillized and unfibrillized Aβ_{1-40} samples, determined from one-dimensional spectra acquired at 9.39 T with magic-angle spinning and proton decoupling

Labeled site	Linewidth (ppm), fibrillized	Linewidth (ppm), unfibrillized
Ala-2 β-carbon	6.1	nd¶
Phe-4 carbonyl	3.5	4.3
Gly-9 α-carbon	3.2	5.3
Val-12 carbonyl	1.7	3.0
Leu-17 carbonyl	1.9	nd
Phe-20 carbonyl	3.4*	nd
Ala-21 β-carbon	3.5†	nd
Val-24 carbonyl	2.9	nd
Ala-30 β-carbon	2.2	6.6
Leu-34 carbonyl	3.2‡	nd
Val-39 carbonyl	3.0 (2.7§)	3.9

*Two partially resolved NMR lines, 2.1 ppm and 2.1 ppm linewidths, 1.5 ppm separation.
†Two partially resolved NMR lines, 2.0 ppm and 2.0 ppm linewidths, 2.0 ppm separation.
‡Two partially resolved NMR lines, 1.3 ppm and 2.6 ppm linewidths, 1.5 ppm separation.
§Sample prepared by incubation in phosphate-buffered saline.
¶nd, Not determined.

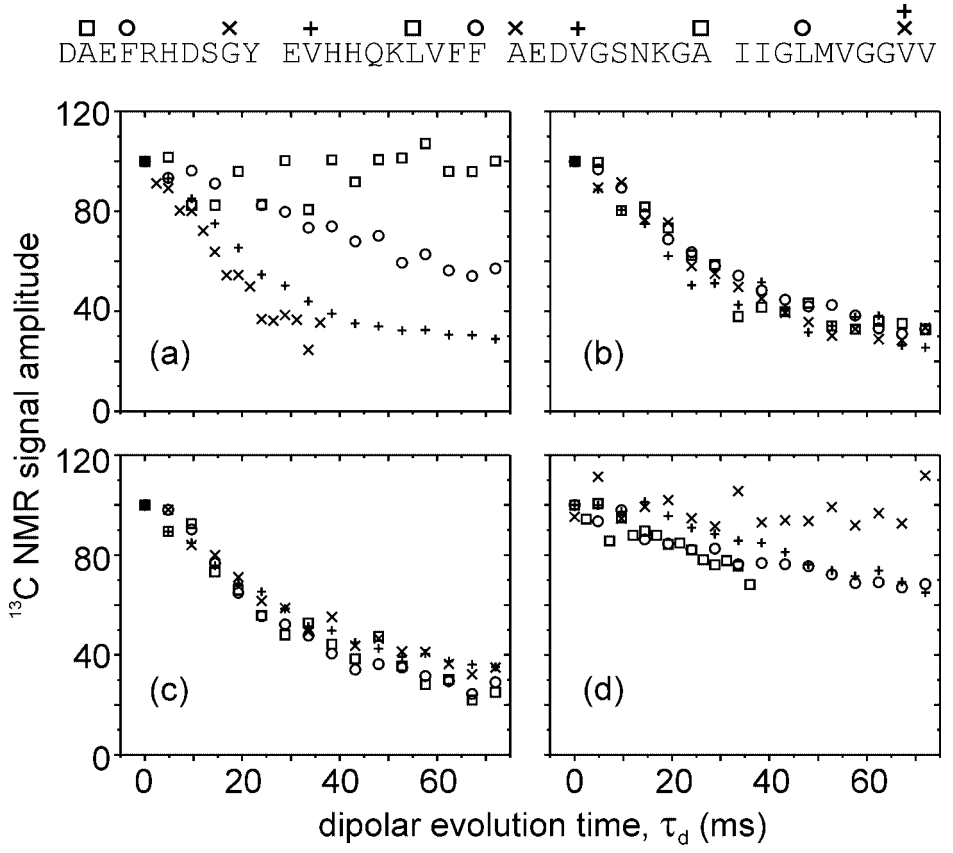

FIGURE 3 Experimental fpRFDR-CT data for fibrillized (*a–c*) and unfibrillized (*d*) ^{13}C-labeled Aβ_{1-40} samples. Labeled residues are indicated by symbols above the amino acid sequence (symbols refer to parts *a*, *b*, and *c*). Data reflect intermolecular dipole-dipole couplings between ^{13}C labels at the following single sites: (*a*) Ala-2 β-carbon (□), Phe-4 carbonyl (○), Gly-9 α-carbon (×), Val-12 carbonyl (+); (*b*) Leu-17 carbonyl (□), Phe-20 carbonyl (○), Ala-21 β-carbon (×), Val-24 carbonyl (+); (*c*) Ala-30 β-carbon (□), Leu-34 carbonyl (○), Val-39 carbonyl (×), Val-39 carbonyl fibrillized from phosphate-buffered saline (+); (*d*) Gly-9 α-carbon (□), Val-12 carbonyl (○), Ala-30 β-carbon (×), Val-39 carbonyl (+). All data were acquired at ^{13}C NMR frequencies of 100.4 or 100.8 MHz, MAS frequency of 20.0 kHz, and nominally identical pulse sequence conditions. All data were acquired with $K = 4$, $M + 2N = 192$, and M ranging from 64 to 184 (see Fig. 1) except data for the Gly-9 α-carbon, for which $K = 2$. All data are normalized to a value of 100 at $\tau_d = 0$. Very similar fpRFDR-CT data, indicating very similar intermolecular ^{13}C-^{13}C distances, are observed for all labeled sites in fibrillized Aβ_{1-40} except sites near the N terminus (Ala-2, Phe-4, Gly-9). Unfibrillized samples exhibit significantly slower signal decays, indicating longer intermolecular ^{13}C-^{13}C distances.

Experimental ^{13}C-^{13}C dipolar recoupling data

Fig. 3, *a* to *c*, shows fpRFDR-CT data for all samples. Data for all fibrillized Aβ_{1-40} samples follow very similar dipolar evolution curves, with the exception of data for the β-carbon of Ala-2 and the carbonyl carbon of Phe-4 (Fig. 3 *a*). Data for these sites decay significantly more slowly with increasing τ_d than data for other labeled sites. Data for all unfibrillized Aβ_{1-40} samples (Fig. 3 *d*) also decay more slowly. Interestingly, fpRFDR-CT data for the carbonyl carbon of Val-39 in two different fibrillized samples, prepared by incubation under quite different conditions of ionic strength and peptide concentration, are not significantly different (Fig. 3 *c*).

Data for the α-carbon of Gly-9 in fibrillized Aβ_{1-40} decay somewhat more rapidly than data for all other sites in fibrillized samples. This observation is discussed below.

In an in-register parallel β-sheet, i.e., a parallel β-sheet in which the backbone amide and carbonyl groups of residue k of one peptide chain are hydrogen-bonded to backbone carbonyl and amide groups of residues $k - 1$ and $k + 1$ of a neighboring chain, the nearest-neighbor distance between the same ^{13}C-labeled sites on different peptide molecules is expected to be 4.8 ± 0.1 Å. The dipole-dipole coupling constant for a pair of ^{13}C nuclei separated by a distance R is $d_{CC} \equiv \gamma^2\hbar/2\pi R^3$,, in which γ is the nuclear magnetogyric ratio. At $R = 4.8$ Å, $d_{CC} = 69$ Hz. In a dipolar recoupling measurement such as fpRFDR-CT, one expects dipolar evolution to occur on the time scale of $(\sigma d_{CC})^{-1}$, in which σ represents the dipolar recoupling efficiency (i.e., the scaling factor of the pulse sequence used to restore dipole-dipole couplings under MAS). For the fpRFDR sequence used in our experiments, $\sigma \approx 0.3$. The experimentally observed

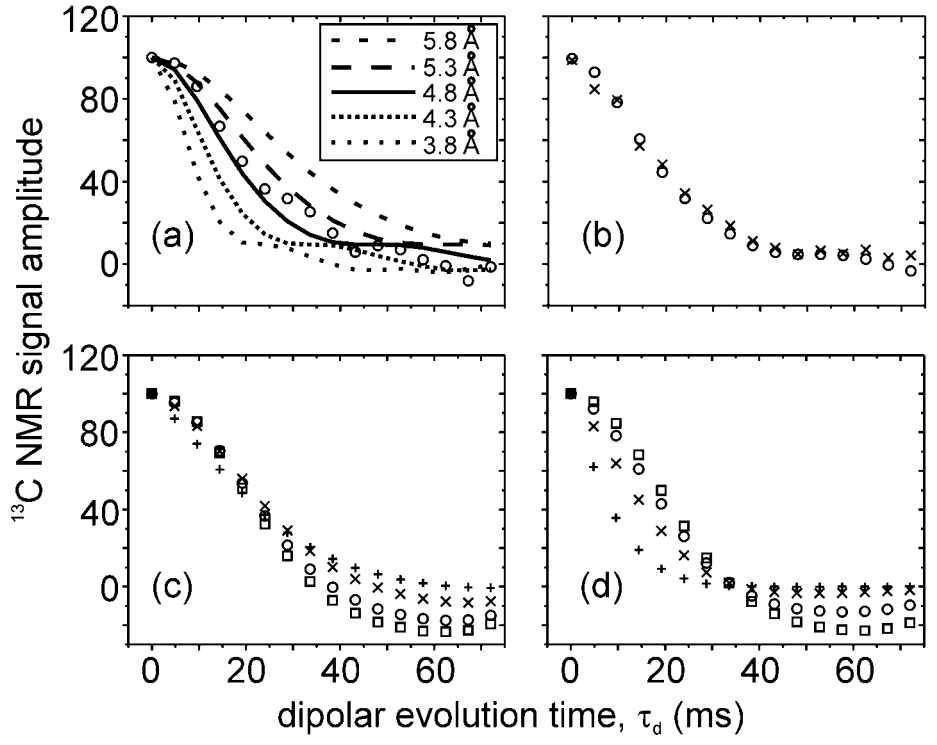

FIGURE 4 Simulated fpRFDR-CT data, normalized to a value of 100 at $\tau_d = 0$. (*a*) Numerical simulations for a linear chain of six ^{13}C spins with the indicated nearest-neighbor distances. ○, Experimental data for fibrillized Aβ_{1-40} with a ^{13}C label at the carbonyl site of Leu-34 after correction for natural-abundance ^{13}C signals (see text). These data are representative of experimental data for ^{13}C-labeled sites from Val-12 through Val-39 (see Fig. 3). Comparison of experimental and simulated data indicates a distance of 4.8 ± 0.5 Å. (*b*) Sensitivity to CSA. Simulations for a linear chain of four ^{13}C spins with a 4.8-Å nearest-neighbor distance and with no CSA (○) or with CSA tensors appropriate for backbone carbonyl sites in a parallel β-sheet (×, see text for CSA parameters). CSA effects are not significant. (*c*) Sensitivity to transverse spin relaxation. Simulations for two ^{13}C spins with a 4.8-Å internuclear distance, including CSA and transverse relaxation (T_2). Results are shown for T_2 values of 1000 ms (□), 100 ms (○), 30 ms (×), and 10 ms (+). (*d*) Simulations for a hypothetical fpRFDR measurement performed in a nonconstant-time manner (i.e., $K = 4$, $N = 0$, and M incremented from 0 to 180). Symbols defined as in part *c*. Use of a constant-time technique reduces the sensitivity of the data to spin relaxation.

time scale for decay of ^{13}C NMR signals from the majority of labeled sites in fibrillized Aβ_{1-40} samples is therefore qualitatively consistent with intermolecular dipole-dipole couplings within a single β-sheet. The fact that quite similar fpRFDR-CT curves are observed for all labeled sites in the range of residues from Val-12 through Val-39 indicates a parallel alignment of neighboring hydrogen-bonded peptide chains in Aβ_{1-40} fibrils, extending over this entire range of residues. A more quantitative analysis of the data, by comparison with numerical simulations, follows.

Simulations of dipolar recoupling data

Fig. 4 *a* shows simulated fpRFDR-CT data for a linear chain of six ^{13}C nuclei with nearest-neighbor internuclear distances from 3.8 to 5.8 Å. The simulated data for distances of ~4.8 Å are in good agreement with experimental data for fibrillized Aβ_{1-40} samples with ^{13}C labels at residues from Val-12 through Val-39, in that the time scale for the decay of ^{13}C NMR signals is roughly 30 ms. Simulated and experimental data differ in that the experimental signal amplitudes at $\tau_d = 72$ ms are ~30% of the amplitudes at $\tau_d = 0$, whereas the simulated data decay to zero. We attribute this difference primarily to signal contributions from natural-abundance ^{13}C nuclei in the experiments. Under the conditions of our fpRFDR-CT measurements on carbonyl-labeled samples, all carbonyl and carboxyl ^{13}C nuclei contribute to the measured signal amplitudes. Based on the amino acid composition and 1.1% natural-abundance level, natural-abundance nuclei account for roughly 35% of the total signal amplitudes at $\tau_d = 0$. Based on the expected density of carbonyl and carboxyl carbon sites in a laminated β-sheet structure (roughly one site per 120 Å^3), one expects ~80% of these natural-abundance ^{13}C nuclei to have no ^{13}C neighbors within a radius of 8 Å. Consequently, most of the natural-abundance ^{13}C NMR signal contribution is expected to decay slowly compared with the maximal value of τ_d in the fpRFDR-CT experiments reported in Fig. 3.

As a representative comparison between experiments and simulations, experimental fpRFDR-CT data for the $A\beta_{1-40}$ fibril sample labeled at the carbonyl site of Leu-34 are replotted in Fig. 4 *a* after correction for natural-abundance ^{13}C signals by subtraction of 30% of the initial signal amplitude and renormalization (i.e., $B(\tau_d) = [A(\tau_d) - 0.3A(0)]/0.7$, in which $A(\tau_d)$ and $B(\tau_d)$ are the uncorrected and corrected fpRFDR-CT amplitudes). The agreement between the corrected experimental data and simulations indicates an intermolecular, internuclear distance of 4.8 ± 0.5 Å.

The contribution of natural-abundance ^{13}C nuclei to fpRFDR-CT data for the β-carbon labeled samples is expected to be similar to that for carbonyl-labeled samples, in agreement with the experimental observation that carbonyl-labeled $A\beta_{1-40}$ fibril samples (except Phe-4) and β-carbon-labeled samples (except Ala-2) exhibit nearly identical fpRFDR-CT curves. Because of the pulsed spin-locking technique used to enhance the signal-to-noise ratio of the fpRFDR-CT measurements (Petkova and Tycko, 2002), natural-abundance aliphatic carbon signals within approximately ±10 ppm of the labeled β-carbon signal contribute to the fpRFDR-CT data. From spectral integrations, we estimate this contribution to be 45% of the total aliphatic carbon signal, or ~50 natural-abundance carbon sites. At 1.1% natural abundance, 50 carbon sites contribute 35% of the ^{13}C NMR signal from a peptide with a single ^{13}C-labeled site.

This intermolecular distance determination by comparison of experimental and simulated fpRFDR-CT data assumes that the idealized simulations in Fig. 4 *a* (see Materials and Methods for simulation details) are an adequate representation of the experimental conditions, apart from the issue of natural-abundance ^{13}C signals discussed above. The simulations in Fig. 4 *a* do not include possible effects of ^{13}C CSA and spin relaxation. The fact that quite similar experimental data are obtained for ^{13}C-labeled carbonyl (large CSA) and methyl (small CSA) sites suggests that CSA effects are unimportant. As further confirmation, Fig. 4 *b* shows the results of simulations for a linear chain of four ^{13}C nuclei with 4.8 Å nearest-neighbor distances, both with and without CSA. These simulations include a numerical calculation of the nuclear spin evolution operator for fpRFDR-CT pulse sequence, explicitly including the time-dependence of the spin Hamiltonian under MAS and the time-dependent ^{13}C rf fields, rather than the time-independent average Hamiltonian treatment used in the simulations in Fig. 4 *a*. CSA parameters are appropriate for experiments on carbonyl-labeled samples (i.e., CSA principal values $\delta_{11} = 70$ ppm, $\delta_{22} = 10$ ppm, and $\delta_{33} = -80$ ppm relative to the carrier frequency; 9.39 *T* static magnetic field; internuclear vectors in the plane of the δ_{11} and δ_{22} principal axes at a 10° angle to the δ_{22} axis). The close agreement between simulated data with and without CSA shows that effects of ^{13}C CSA are unimportant, and the average Hamiltonian treatment is sufficient, under the experimental conditions.

Effects of transverse ^{13}C spin relaxation on fpRFDR-CT data are shown in the simulations in Fig. 4 *c*, which were carried out for a two-spin system with an internuclear distance of 4.8 Å using an approximate treatment of spin relaxation (see Materials and Methods) and including CSA as described above. Transverse relaxation times T_2 as short as 10 ms do not affect the initial signal decay rates strongly, although the apparent plateau value of the signal amplitude at larger τ_d values may be affected. In contrast, transverse spin relaxation has a much greater effect on initial signal decay rates in a dipolar recoupling measurements performed in a nonconstant time manner, as shown in the simulations in Fig. 4 *d*.

Transverse spin relaxation rates were measured experimentally for several $A\beta_{1-40}$ samples, using a Carr-Purcell echo train technique under MAS at $\nu_R = 20.0$ kHz with a 200 μs spacing between ^{13}C π pulses in the echo train. Experimental relaxation curves were biexponential (see Materials and Methods). In fibrillized $A\beta_{1-40}$, values of the relaxation times and signal fractions determined by a least-squares fit to the Carr-Purcell data were: $(T_{2a}, f_a, T_{2b}, f_b) =$ (54 ms, 0.66, 6 ms, 0.34) for the carbonyl carbon of Phe-4; (81 ms, 0.77, 8 ms, 0.23) for the carbonyl carbon of Val-12; (66 ms, 0.73, 5 ms, 0.27) for the β-carbon of Ala-30; (61 ms, 0.75, 7 ms, 0.25) for the carbonyl carbon of Val-39. Times for decay of the ^{13}C NMR signal to $1/e$ of its initial value were 32, 60, 45, and 44 ms, respectively. According to Fig. 4 *c*, these relaxation times are in a regime where experimental fpRFDR-CT data are not strongly affected.

DISCUSSION

$A\beta_{1-40}$ molecules have an in-register parallel organization in amyloid fibrils

The main result of the fpRFDR-CT data reported above is that $A\beta_{1-40}$ molecules have a parallel alignment within the β-sheets in the amyloid fibrils. The parallel alignment spans a region that includes residues Val-12 through Val-39. This result follows from the observation of intermolecular ^{13}C-^{13}C dipole-dipole couplings that indicate intermolecular distances of 4.8 ± 0.5 Å between single-site ^{13}C labels at eight positions (Fig. 3, *a–c*), including multiple sites in each of the two hydrophobic segments of $A\beta_{1-40}$ (residues 17–21 and 29–40) and sites preceding (Val-12) and separating (Val-24) the two hydrophobic segments. The nearest-neighbor intermolecular distance between backbone carbonyl carbons is 4.8 ± 0.1 Å in both parallel and antiparallel β-sheets, so a single intermolecular distance measurement would not be sufficient to identify the structural organization of the β-sheets. However, as should be clear from inspection of the schematic parallel β-sheet structure in Fig. 5, the experimental measurement of the same intermolecu-

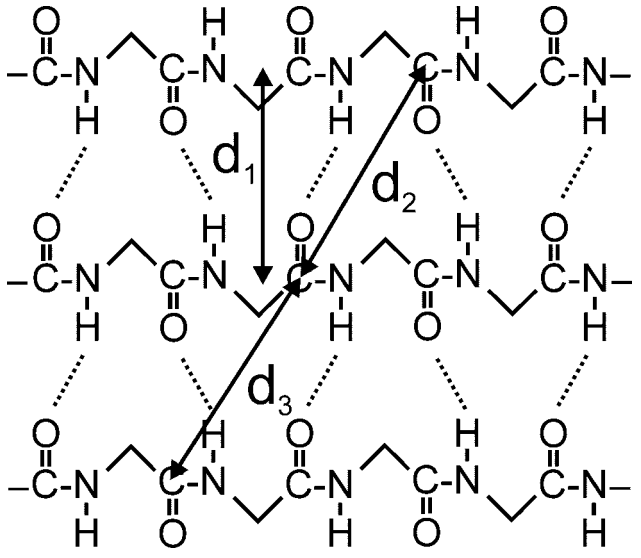

FIGURE 5 Schematic representation of a parallel β-sheet in an amyloid fibril. Dashed lines indicate intermolecular hydrogen bonds. For a peptide with a ^{13}C label at a single backbone carbonyl site, d_1 is the intermolecular nearest-neighbor distance in an in-register parallel structure, whereas d_2 and d_3 are the distances in an out-of-register structure in which the hydrogen bonding pattern is shifted by one residue. Typically, $d_1 \approx 4.8$ Å, $d_2 \approx 5.1$ Å, and $d_3 \approx 6.6$ Å.

lar distance between single ^{13}C labels at multiple sites in $A\beta_{1-40}$ fibrils establishes the parallel organization.

The fpRFDR-CT data do not imply (nor do we mean to suggest) that the entire segment from Val-12 through Val-39 exists as a single β-strand, but only that the alignment of neighboring peptide chains is parallel. These data alone do not rule out non-β-strand conformations at the ^{13}C-labeled residues in this segment or at other residues in this segment. While the major structural elements of $A\beta_{1-40}$ fibrils are parallel β-sheets, the peptide chain does not necessarily form a single β-sheet. Non-β-strand backbone conformations in certain segments, such as the bends or loops observed in the β-sheet structures of pertactin (Emsley et al., 1996) and pectate lyase C (Yoder et al., 1993), are possible and indeed are indicated by solid-state NMR chemical shift and torsion angle measurements on $A\beta_{1-40}$ fibrils (A. T. Petkova, Y. Ishii, O. N. Antzutkin, J. J. Balbach, R. D. Leapman, and R. Tycko, submitted manuscript). Non-β-strand segments are included in several recent structural models of Aβ fibrils (Chaney et al., 1998; George and Howlett, 1999; Li et al., 1999; Tjernberg et al., 1999; Lazo and Downing, 1998).

The fpRFDR-CT data are primarily sensitive to pairwise ^{13}C-^{13}C dipole-dipole couplings. Therefore, these data alone do not firmly establish an extended parallel β-sheet structure, as opposed to a hypothetical structure in which the $A\beta_{1-40}$ molecules form parallel dimers (or perhaps higher oligomers), which then align in an antiparallel (or perhaps staggered) manner in the β-sheets. The existence of an extended parallel β-sheet structure, in which the parallel alignment persists over at least four (and probably many more) molecules within a single β-sheet, has been established by our earlier multiple quantum NMR measurements on the $A\beta_{1-40}$ fibril samples with ^{13}C labels at the β-carbons of Ala-21 and Ala-30 (Antzutkin et al., 2000).

The fpRFDR-CT data are consistent with an in-register parallel β-sheet structure. In an in-register parallel β-sheet, the backbone amide and carbonyl groups of residue k of one peptide molecule are hydrogen-bonded to the carbonyl and amide groups of residues $k - 1$ and $k + 1$ of a neighboring molecule. The nearest-neighbor intermolecular distances between ^{13}C labels at a single backbone carbonyl site are then 4.8 $\pm$ 0.1 Å (d_1 in Fig. 5). The nearest-neighbor intermolecular distances between ^{13}C labels at β-carbon sites are also 4.8 $\pm$ 0.1 Å in an in-register parallel structure. If the hydrogen-bonding pattern were shifted by one residue, the nearest-neighbor distances between labeled carbonyl sites would alternate between roughly 5.1 and 6.6 Å (d_2 and d_3 in Fig. 5), based on an examination of extended parallel β-sheets in proteins of known structure (Emsley et al., 1996). The fpRFDR-CT data on carbonyl-labeled $A\beta_{1-40}$ samples therefore do not rule out a shift by one residue, although a shift by more than one residue would lead to longer distances between labeled sites that would be incompatible with these data. However, because of the additional displacements of C_β carbons above and below the plane of the peptide backbones in β-sheets, the nearest-neighbor distances between ^{13}C labels in the samples with labels at β-carbons of Ala-21 and Ala-30 would be $\sim$7.4 Å if these residues were in parallel β-sheets with a one-residue shift of the hydrogen bonds. The fpRFDR-CT data for these two samples are only consistent with an in-register parallel structure. In addition, multiple quantum ^{13}C NMR measurements on $A\beta_{1-40}$ fibrils are not consistent with a shifted structure but are consistent with an in-register structure (Antzutkin et al., 2000), implying that the parallel alignment in $A\beta_{1-40}$ fibrils is in-register. In particular, the amplitudes of 3- and 4-quantum signals, relative to the amplitude of the 2-quantum signal, are greater in experimental multiple quantum spectra than in simulated spectra for a shifted parallel β-sheet structure. (Experimental 2-, 3-, and 4-quantum amplitudes at multiple quantum excitation time τ_{MQ} = 14.4 ms are in a 1.00:0.23:0.07 ratio for $A\beta_{1-40}$ fibrils with ^{13}C labels at β-carbons of Ala-21 or Ala-30. Simulated 2-, 3-, and 4-quantum amplitudes for a structure with a one-residue shift are in a 1.00:0.13:0.04 ratio.)

The possible dependence of the β-sheet organization on ionic strength was investigated by comparison of fpRFDR-CT data for $A\beta_{1-40}$ samples labeled at the carbonyl site of Val-39 and incubated at either low ionic strength or in phosphate-buffered saline. The data are nearly indistinguishable (Fig. 3 *c*), indicating that the parallel β-sheet organization observed in fpRFDR-CT and multiple

quantum NMR measurements is not restricted to low ionic strength conditions.

The fpRFDR-CT data cannot be explained by ^{13}C-^{13}C couplings between molecules in different β-sheet laminae or in different protofilaments. Within the context of a laminated β-sheet structural model (Sunde and Blake, 1998; Sunde et al., 1997), x-ray diffraction measurements indicate an average spacing of ~9 Å between laminae (Malinchik et al., 1998). Although shorter interlaminar distances might conceivably occur at specific sites, the observation of nearly indistinguishable fpRFDR-CT data at multiple sites spanning residues Val-12 through Val-39 shows that couplings between laminae are not important in the experiments described above.

One might propose that close contacts between different protofilaments within a fibril could produce the ^{13}C-^{13}C couplings observed in fpRFDR-CT data for a sample in which the ^{13}C labels happen to be at a point of contact between the protofilaments. To be consistent with the 4.8 ± 0.5 Å internuclear distances observed in the experiments, the labeled site would have to be a sidechain carbon (such as the β-carbon of Ala-21 or Ala-30) or the carbonyl carbon of a residue that either possesses a small sidechain (i.e., alanine or glycine) or is surrounded by other residues with small sidechains. Otherwise, steric effects would require the distances between ^{13}C labels in different protofilaments to be greater than the experimental values. Multiple quantum NMR data on $A\beta_{1-40}$ samples with labels at β-carbons of Ala-21 and Ala-30 require that at least four ^{13}C labels be in close proximity (Antzutkin et al., 2000). Additionally, none of the carbonyl-labeled residues in our fpRFDR-CT measurements possesses a small sidechain or is surrounded by residues with small sidechains. Thus, it appears extremely improbable that contacts between different protofilaments could account for any of the fpRFDR-CT data. It is impossible for such contacts to account for all of the data.

N-terminal segment of $A\beta_{1-40}$ is disordered in the amyloid fibrils

Solid-state NMR linewidths are correlated with structural order. Structurally ordered peptides in rigid noncrystalline environments such as amyloid fibrils (Balbach et al., 2000) or frozen solutions (Weliky et al., 1999) typically exhibit ^{13}C MAS NMR linewidths in the 1.0 to 2.5 ppm range. Linewidths for ^{13}C-labeled sites from Val-12 through Val-39 in fibrillized $A\beta_{1-40}$ (Table 1) are generally consistent with an ordered structure. ^{13}C NMR linewidths in unfibrillized $A\beta_{1-40}$ samples are significantly larger than in fibrillized samples. Although overall linewidths for ^{13}C labels at carbonyl sites of Phe-20 and Leu-34 and the β-carbon site of Ala-21 in fibrillized $A\beta_{1-40}$ are greater than 3.0 ppm, in these three cases (but in no other cases for samples investigated in this paper) the ^{13}C NMR lineshapes clearly show two partially resolved peaks with individual widths in the 1.3 to 2.6 ppm range. Linewidths for the β-carbon of Ala-2, the carbonyl carbon of Phe-4, and the α-carbon of Gly-9 in fibrillized samples are anomalously large, suggesting more structural disorder at these sites than at ^{13}C-labeled sites from Val-12 through Val-39.

The fpRFDR-CT data for the β-carbon of Ala-2 and the carbonyl carbon of Phe-4 (Fig. 3 *a*) decay significantly more slowly than data for all other sites in $A\beta_{1-40}$ fibrils and indicate average intermolecular ^{13}C-^{13}C distances greater than 7 Å. Data for Ala-2 and Phe-4 in $A\beta_{1-40}$ fibrils are similar to data for unfibrillized samples (Fig. 3 *d*). In multiple quantum NMR measurements, high-order multiple quantum signals were not observed for $A\beta_{1-40}$ fibrils labeled at the β-carbon of Ala-2 (Antzutkin et al., 2000), consistent with the weak ^{13}C-^{13}C couplings revealed by the fpRFDR-CT data. The fpRFDR-CT data for the α-carbon of Gly-9 decay more quickly than data for all other sites and indicate an intermolecular ^{13}C-^{13}C distance of 4.5 ± 0.5 Å.

Together, the linewidth and fpRFDR-CT data indicate that the N-terminal segment of $A\beta_{1-40}$ is structurally disordered in the fibrils. The disordered segment includes Ala-2 and Phe-4 and apparently includes Gly-9, although the average nearest-neighbor intermolecular distance for Gly-9 α-carbons is somewhat less than intermolecular distances for labeled sites in the ordered region of the fibrils. The disordered segment terminates before Val-12. A structurally disordered N-terminal segment is consistent with previous observations that the N-terminal residues in $A\beta_{1-42}$ fibrils are subject to proteolysis in vivo (Roher et al., 1993) and in vitro (Kheterpal et al., 2001), as well as the observation that ~30% of the backbone amide sites in $A\beta_{1-40}$ fibrils are accessible to relatively rapid hydrogen exchange (Kheterpal et al., 2000).

Structural disorder in the N-terminal segment of $A\beta_{1-40}$ is possible despite the structural order and presumed tight packing of residues 12 to 40 because the N-terminal segment is free to occupy three spatial dimensions, whereas residues 12 to 40 are restricted to an essentially two-dimensional structure.

Comparisons with related structural data and structural models

The fpRFDR-CT data for the ordered region of $A\beta_{1-40}$ fibrils reported above are highly reminiscent of solid-state NMR data reported by Lynn, Meredith, Botto, and coworkers for $A\beta_{10-35}$ fibrils (Benzinger et al., 1998, 2000; Burkoth et al., 2000), in which the DRAWS dipolar recoupling technique (Gregory et al., 1995, 1998) was used to measure intermolecular ^{13}C-^{13}C dipole-dipole couplings in samples with single backbone carbonyl labels. From their DRAWS data, Lynn, Meredith, Botto, and coworkers conclude that the β-sheets in $A\beta_{10-35}$ fibrils have an in-register parallel organization. Antzutkin and colleagues report fpRFDR-CT data for both $A\beta_{10-35}$ and $A\beta_{1-42}$ fibrils that

also indicate parallel alignment of neighboring peptide chains within the β-sheets in these fibrils (O. N. Antzutkin, R. D. Leapman, N. W. Rizzo, J. J. Balbach, and R. Tycko. 2002, submitted manuscript). Thus, the β-sheet structures in $A\beta_{10-35}$, $A\beta_{1-40}$, and $A\beta_{1-42}$ fibrils are quite similar.

Lynn, Meredith, Botto, and coworkers propose a structural model for $A\beta_{10-35}$ fibrils in which the entire peptide chain adopts a β-strand conformation (Burkoth et al., 2000). This model represents a combination of solid-state NMR, neutron scattering, and other physical measurements on a truncated peptide. Their data are, in the main, consistent with the data on $A\beta_{1-40}$ reported above, which indicate that residues 12 through 39 have an in-register parallel alignment and the N-terminal segment is disordered.

Antiparallel β-sheets have been identified in $A\beta_{16-22}$ (Balbach et al., 2000) and $A\beta_{34-42}$ (Lansbury et al., 1995) fibrils, based on solid-state NMR measurements. The supramolecular structures of amyloid fibrils are therefore diverse and are not uniquely determined at the level of short (e.g., seven-residue) sequences. At the molecular level, a universal structure for amyloid fibrils does not exist. Given the diversity of peptides and proteins that form amyloid fibrils, the absence of a universal molecular structure may not be surprising.

Several structural models for full-length Aβ fibrils containing antiparallel β-sheets have been proposed (Chaney et al., 1998; George and Howlett, 1999; Li et al., 1999; Tjernberg et al., 1999; Lazo and Downing, 1998). The choice of antiparallel β-sheets in these models is apparently based primarily on infrared spectroscopy (as well as the solid-state NMR data for $A\beta_{34-42}$). Although the observation of a strong amide I band near 1630 cm^{-1} and a weaker band near 1690 cm^{-1} in infrared spectra of amyloid fibrils has been interpreted as evidence for antiparallel β-sheets in amyloid fibrils (Hilbich et al., 1991; Fraser et al., 1992; Conway et al., 2000), recent measurements on parallel β-sheet proteins (Khurana and Fink, 2000) indicate that these amide I signals are not absolutely unique signatures of antiparallel β-sheets. X-ray diffraction data do not clearly distinguish parallel and antiparallel β-sheet structures in amyloid fibrils (Inouye et al., 1993; Blake and Serpell, 1996).

Certain structural models for Aβ fibrils include a β-hairpin with intramolecular backbone hydrogen bonding between β-strand segments on either side of a β-turn located between Val-24 and Asn27 (Lazo and Downing, 1998), Gly-25 and Lys-28 (Li et al., 1999; George and Howlett, 1999), or Ile32 and Gly-37 (Tjernberg et al., 1999). Intramolecular hydrogen bonding of β-strand segments appears incompatible with the in-register parallel alignment and 4.8 ± 0.5 Å nearest-neighbor intermolecular distances indicated by our solid-state NMR data, as our own attempts to construct a plausible structural model that includes intramolecular hydrogen bonding (as in a true β-hairpin) and also satisfies the constraints imposed by the solid-state NMR data have been unsuccessful.

The significance of the various possible intermolecular and intramolecular interactions in stabilizing amyloid fibril structures is an important issue. The experimental observation of an in-register parallel β-sheet organization in amyloid fibrils formed by peptides with asymmetrically distributed hydrophobic segments, such as $A\beta_{1-40}$, $A\beta_{10-35}$, and $A\beta_{1-42}$, suggests that intermolecular hydrophobic interactions play a dominant role in determining the supramolecular structure, because an in-register parallel organization juxtaposes hydrophobic residues while an antiparallel organization does not (Antzutkin et al., 2000; Balbach et al., 2000). An in-register parallel organization might lead to destabilizing intermolecular electrostatic interactions among charged residues, but these might be reduced by favorable electrostatic interactions between adjacent β-sheet laminae, by favorable intramolecular electrostatic interactions, or by incorporation of counterions into the fibril.

The intermolecular distance constraints reported above, as well as structural constraints from other solid-state NMR measurements (Antzutkin et al., 2000; A. T. Petkova, Y. Ishii, O. N. Antzutkin, J. J. Balbach, R. D. Leapman, and R. Tycko, submitted manuscript), should facilitate the development of more accurate structural models for $A\beta_{1-40}$ fibrils and the development of a more complete understanding of the interactions that stabilize amyloid fibril structures.

REFERENCES

Antzutkin, O. N., J. J. Balbach, R. D. Leapman, N. W. Rizzo, J. Reed, and R. Tycko. 2000. Multiple quantum solid-state NMR indicates a parallel, not antiparallel, organization of beta-sheets in Alzheimer's beta-amyloid fibrils. *Proc. Natl. Acad. Sci. U. S. A.* 97:13045–13050.

Balbach, J. J., Y. Ishii, O. N. Antzutkin, R. D. Leapman, N. W. Rizzo, F. Dyda, J. Reed, and R. Tycko. 2000. Amyloid fibril formation by A beta(16–22), a seven-residue fragment of the Alzheimer's beta-amyloid peptide, and structural characterization by solid-state NMR. *Biochemistry.* 39:13748–13759.

Bennett, A. E., J. H. Ok, R. G. Griffin, and S. Vega. 1992. Chemical-shift correlation spectroscopy in rotating solids: radio frequency-driven dipolar recoupling and longitudinal exchange. *J. Chem. Phys.* 96: 8624–8627.

Bennett, A. E., C. M. Rienstra, J. M. Griffiths, W. G. Zhen, P. T. Lansbury, and R. G. Griffin. 1998. Homonuclear radio frequency-driven recoupling in rotating solids. *J. Chem. Phys.* 108:9463–9479.

Benzinger, T. L. S., D. M. Gregory, T. S. Burkoth, H. Miller-Auer, D. G. Lynn, R. E. Botto, and S. C. Meredith. 1998. Propagating structure of Alzheimer's beta-amyloid((10–35)) is parallel beta-sheet with residues in exact register. *Proc. Natl. Acad. Sci. U. S. A.* 95:13407–13412.

Benzinger, T. L. S., D. M. Gregory, T. S. Burkoth, H. Miller-Auer, D. G. Lynn, R. E. Botto, and S. C. Meredith. 2000. Two-dimensional structure of beta-amyloid(10–35) fibrils. *Biochemistry.* 39:3491–3499.

Blackley, H. K. L., G. H. W. Sanders, M. C. Davies, C. J. Roberts, S. J. B. Tendler, and M. J. Wilkinson. 2000. In-situ atomic force microscopy study of beta-amyloid fibrillization. *J. Mol. Biol.* 298:833–840.

Blake, C., and L. Serpell. 1996. Synchrotron X-ray studies suggest that the core of the transthyretin amyloid fibril is a continuous beta-sheet helix. *Structure.* 4:989–998.

Burkoth, T. S., T. L. S. Benzinger, V. Urban, D. M. Morgan, D. M. Gregory, P. Thiyagarajan, R. E. Botto, S. C. Meredith, and D. G. Lynn. 2000. Structure of the beta-amyloid((10–35)) fibril. *J. Am. Chem. Soc.* 122:7883–7889.

Carr, H. Y., and E. M. Purcell. 1954. Effects of diffusion on free precession in nuclear magnetic resonance experiments. *Phys. Rev.* 94:630–638.

Chaney, M. O., S. D. Webster, Y. M. Kuo, and A. E. Roher. 1998. Molecular modeling of the A beta 1–42 peptide from Alzheimer's disease. *Protein Eng.* 11:761–767.

Chiti, F., P. Webster, N. Taddei, A. Clark, M. Stefani, G. Ramponi, and C. M. Dobson. 1999. Designing conditions for in vitro formation of amyloid protofilaments and fibrils. *Proc. Natl. Acad. Sci. U. S. A.* 96:3590–3594.

Conway, K. A., J. D. Harper, and P. T. Lansbury. 2000. Fibrils formed in vitro from alpha-synuclein and two mutant forms linked to Parkinson's disease are typical amyloid. *Biochemistry.* 39:2552–2563.

Costa, P. R., D. A. Kocisko, B. Q. Sun, P. T. Lansbury, and R. G. Griffin. 1997. Determination of peptide amide configuration in a model amyloid fibril by solid-state NMR. *J. Am. Chem. Soc.* 119:10487–10493.

Emsley, P., I. G. Charles, N. F. Fairweather, and N. W. Isaacs. 1996. Structure of Bordetella pertussis virulence factor P.69 pertactin. *Nature.* 381:90–92.

Fraser, P. E., J. T. Nguyen, H. Inouye, W. K. Surewicz, D. J. Selkoe, M. B. Podlisny, and D. A. Kirschner. 1992. Fibril formation by primate, rodent, and Dutch-hemorrhagic analogs of Alzheimer amyloid beta-protein. *Biochemistry.* 31:10716–10723.

Fraser, P. E., J. T. Nguyen, W. K. Surewicz, and D. A. Kirschner. 1991. Ph-Dependent structural transitions of Alzheimer amyloid peptides. *Biophys. J.* 60:1190–1201.

George, A. R., and D. R. Howlett. 1999. Computationally derived structural models of the beta-amyloid found in Alzheimer's disease plaques and the interaction with possible aggregation inhibitors. *Biopolymers.* 50:733–741.

Goldsbury, C., J. Kistler, U. Aebi, T. Arvinte, and G. J. S. Cooper. 1999. Watching amyloid fibrils grow by time-lapse atomic force microscopy. *J. Mol. Biol.* 285:33–39.

Goldsbury, C. S., S. Wirtz, S. A. Muller, S. Sunderji, P. Wicki, U. Aebi, and P. Frey. 2000. Studies on the in vitro assembly of A beta 1–40: implications for the search for A beta fibril formation inhibitors. *J. Struct. Biol.* 130:217–231.

Gregory, D. M., T. L. S. Benzinger, T. S. Burkoth, H. Miller-Auer, D. G. Lynn, S. C. Meredith, and R. E. Botto. 1998. Dipolar recoupling NMR of biomolecular self-assemblies: determining inter- and intrastrand distances in fibrilized Alzheimer's beta-amyloid peptide. *Solid State Nucl. Magn. Reson.* 13:149–166.

Gregory, D. M., D. J. Mitchell, J. A. Stringer, S. Kiihne, J. C. Shiels, J. Callahan, M. A. Mehta, and G. P. Drobny. 1995. Windowless dipolar recoupling: the detection of weak dipolar couplings between spin-1/2 nuclei with large chemical shift anisotropies. *Chem. Phys. Lett.* 246: 654–663.

Griffin, R. G. 1998. Dipolar recoupling in MAS spectra of biological solids. *Nat. Struct. Biol.* 5:508–512.

Griffiths, J. M., T. T. Ashburn, M. Auger, P. R. Costa, R. G. Griffin, and P. T. Lansbury. 1995. Rotational resonance solid-state NMR elucidates a structural model of pancreatic amyloid. *J. Am. Chem. Soc.* 117:3539–3546.

Gullion, T., D. B. Baker, and M. S. Conradi. 1990. New, compensated Carr-Purcell sequences. *J. Magn. Reson.* 89:479–484.

Gullion, T., and J. Schaefer. 1989. Rotational-echo double-resonance NMR. *J. Magn. Reson.* 81:196–200.

Gullion, T., and S. Vega. 1992. A simple magic angle spinning NMR experiment for the dephasing of rotational echoes of dipolar coupled homonuclear spin pairs. *Chem. Phys. Lett.* 194:423–428.

Haeberlen, U., and J. S. Waugh. 1968. Coherent averaging effects in magnetic resonance. *Phys. Rev.* 175:453–467.

Harper, J. D., C. M. Lieber, and P. T. Lansbury. 1997. Atomic force microscopic imaging of seeded fibril formation and fibril branching by the Alzheimer's disease amyloid-beta protein. *Chem. Biol.* 4:951–959.

Harper, J. D., S. S. Wong, C. M. Lieber, and P. T. Lansbury. 1999. Assembly of A beta amyloid protofibrils: an in vitro model for a possible early event in Alzheimer's disease. *Biochemistry.* 38:8972–8980.

Hilbich, C., B. Kisterswoike, J. Reed, C. L. Masters, and K. Beyreuther. 1991. Aggregation and secondary structure of synthetic amyloid βA4 peptides of Alzheimer's disease. *J. Mol. Biol.* 218:149–163.

Inouye, H., P. E. Fraser, and D. A. Kirschner. 1993. Structure of beta-crystallite assemblies formed by Alzheimer beta-amyloid protein analogs: analysis by x-ray-diffraction. *Biophys. J.* 64:502–519.

Ishii, Y. 2001. C-13-C-13 dipolar recoupling under very fast magic angle spinning in solid-state nuclear magnetic resonance: applications to distance measurements, spectral assignments, and high-throughput secondary-structure determination. *J. Chem. Phys.* 114:8473–8483.

Ishii, Y., J. J. Balbach, and R. Tycko. 2001a. Measurement of dipole-coupled lineshapes in a many-spin system by constant-time two-dimensional solid-state NMR with high-speed magic-angle spinning. *Chem. Phys.* 266:231–236.

Ishii, Y., J. P. Yesinowski, and R. Tycko. 2001b. Sensitivity enhancement in solid-state C-13 NMR of synthetic polymers and biopolymers by H-1 NMR detection with high-speed magic angle spinning. *J. Am. Chem. Soc.* 123:2921–2922.

Jimenez, J. L., J. L. Guijarro, E. Orlova, J. Zurdo, C. M. Dobson, M. Sunde, and H. R. Saibil. 1999. Cryo-electron microscopy structure of an SH3 amyloid fibril and model of the molecular packing. *EMBO J.* 18:815–821.

Kheterpal, I., A. Williams, C. Murphy, B. Bledsoe, and R. Wetzel. 2001. Structural features of the A beta amyloid fibril elucidated by limited proteolysis. *Biochemistry.* 40:11757–11767.

Kheterpal, I., S. Zhou, K. D. Cook, and R. Wetzel. 2000. A beta amyloid fibrils possess a core structure highly resistant to hydrogen exchange. *Proc. Natl. Acad. Sci. U. S. A.* 97:13597–13601.

Khurana, R., and A. L. Fink. 2000. Do parallel beta-helix proteins have a unique fourier transform infrared spectrum? *Biophys. J.* 78:994–1000.

Lansbury, P. T., P. R. Costa, J. M. Griffiths, E. J. Simon, M. Auger, K. J. Halverson, D. A. Kocisko, Z. S. Hendsch, T. T. Ashburn, R. G. S. Spencer, B. Tidor, and R. G. Griffin. 1995. Structural model for the beta-amyloid fibril based on interstrand alignment of an antiparallel-sheet comprising a C-terminal peptide. *Nat. Struct. Biol.* 2:990–998.

Lazo, N. D., and D. T. Downing. 1998. Amyloid fibrils may be assembled from beta-helical protofibrils. *Biochemistry.* 37:1731–1735.

Li, L. P., T. A. Darden, L. Bartolotti, D. Kominos, and L. G. Pedersen. 1999. An atomic model for the pleated beta-sheet structure of A beta amyloid protofilaments. *Biophys. J.* 76:2871–2878.

Malinchik, S. B., H. Inouye, K. E. Szumowski, and D. A. Kirschner. 1998. Structural analysis of Alzheimer's β(1–40) amyloid: protofilament assembly of tubular fibrils. *Biophys. J.* 74:537–545.

Petkova, A. T., and R. Tycko. 2002. Sensitivity enhancement in structural measurements by solid-state NMR through pulsed spin locking. *J. Magn. Reson.* 155:293–299.

Roher, A. E., J. D. Lowenson, S. Clarke, C. Wolkow, R. Wang, R. J. Cotter, I. M. Reardon, H. A. Zurcherneely, R. L. Heinrikson, M. J. Ball, and B. D. Greenberg. 1993. Structural alterations in the peptide backbone of beta-amyloid core protein may account for its deposition and stability in Alzheimers-disease. *J. Biol. Chem.* 268:3072–3083.

Serpell, L. C., C. C. F. Blake, and P. E. Fraser. 2000. Molecular structure of a fibrillar Alzheimer's A beta fragment. *Biochemistry.* 39: 13269–13275.

Serpell, L. C., and J. M. Smith. 2000. Direct visualisation of the beta-sheet structure of synthetic Alzheimer's amyloid. *J. Mol. Biol.* 299:225–231.

Stine, W. B., S. W. Snyder, U. S. Ladror, W. S. Wade, M. F. Miller, T. J. Perun, T. F. Holzman, and G. A. Krafft. 1996. The nanometer-scale structure of amyloid-beta visualized by atomic force microscopy. *J. Protein Chem.* 15:193–203.

Storey, E., and R. Cappai. 1999. The amyloid precursor protein of Alzheimer's disease and the Aβ peptide. *Neuropathol. Appl. Neurobiol.* 25:81–97.

Sunde, M., and C. C. F. Blake. 1998. From the globular to the fibrous state: protein structure and structural conversion in amyloid formation. *Q. Rev. Biophys.* 31:1–39.

Sunde, M., L. C. Serpell, M. Bartlam, P. E. Fraser, M. B. Pepys, and C. C. F. Blake. 1997. Common core structure of amyloid fibrils by synchrotron x-ray diffraction. *J. Mol. Biol.* 273:729–739.

Tjernberg, L. O., D. J. E. Callaway, A. Tjernberg, S. Hahne, C. Lilliehook, L. Terenius, J. Thyberg, and C. Nordstedt. 1999. A molecular model of Alzheimer amyloid beta-peptide fibril formation. *J. Biol. Chem.* 274: 12619–12625.

Tycko, R. 2000. Solid-state NMR as a probe of amyloid fibril structure. *Curr. Opin. Chem. Biol.* 4:500–506.

Tycko, R. 2001a. Biomolecular solid-state NMR: advances in structural methodology and applications to peptide and protein fibrils. *Annu. Rev. Phys. Chem.* 52:575–606.

Tycko, R. 2001b. Solid-state nuclear magnetic resonance techniques for structural studies of amyloid fibrils. *In* Methods in Enzymology. vol. 339. T. L. James, V. Dötsch, and U. Schmitz, editors. Academic Press, San Diego, CA. 390–413.

Tycko, R., and G. Dabbagh. 1990. Measurement of nuclear magnetic dipole-dipole couplings in magic angle spinning NMR. *Chem. Phys. Lett.* 173:461–465.

Weliky, D. P., A. E. Bennett, A. Zvi, J. Anglister, P. J. Steinbach, and R. Tycko. 1999. Solid-state NMR evidence for an antibody-dependent conformation of the V3 loop of HIV-1 gp120. *Nat. Struct. Biol.* 6:141–145.

Yoder, M. D., N. T. Keen, and F. Jurnak. 1993. New domain motif: the structure of pectatelyase-C, a secreted plant virulence factor. *Science.* 260:1503–1507.